A Nelder–Mead algorithm-based inverse transient analysis for leak detection and sizing in a single pipe

Oussama Choura, Caterina Capponi, Silvia Meniconi, Sami Elaoud and Bruno Brunone

ABSTRACT

In this paper the results of an experimental validation of a technique for leak detection in polymeric pipes based on the inverse transient analysis (ITA) are presented. In the proposed ITA the Nelder–Mead algorithm is used as a calibration tool. Experimental tests have been carried out in an intact and leaky high-density polyethylene (HDPE) single pipe installed at the Water Engineering Laboratory (WEL) of the University of Perugia, Italy. Transients have been generated by the fast and complete closure of a valve placed at the downstream end section of the pipe. In the first phase of the calibration procedure, the proposed algorithm has been used to estimate both the viscoelastic parameters of a generalized Kelvin–Voigt model and the unsteady-state friction coefficient, by minimizing the difference between the numerical and experimental results. In the second phase of the procedure, the calibrated model allowed the evaluation of leak size and location with an acceptable accuracy. Precisely, in terms of leak location the relative error was smaller than 5%.

Key words | inverse transient analysis, leak detection, Nelder–Mead algorithm, unsteady-state friction, viscoelasticity

Oussama Choura (corresponding author)
Sami Elaoud
Laboratory of Applied Fluid Mechanics, Process Engineering and Environment,
National School of Engineering of Sfax,
3038 Sfax,
Tunisia
E-mail: *oussema.choura@enis.tn*

Oussama Choura
Caterina Capponi
Silvia Meniconi
Bruno Brunone
Dipartimento di Ingegneria Civile ed Ambientale,
The University of Perugia,
Via G. Duranti 93, 06125 Perugia,
Italy

HIGHLIGHTS

- An inverse transient analysis, based on the Nelder–Mead algorithm and laboratory data, is used for viscoelastic parameter estimation of polymeric pipes.
- The same approach is followed for evaluating leak location and size.
- The effect of several parameters, such as the unsteady-state friction, the length in time of the pressure signal, and the location and number of the measurement sections is analyzed.

INTRODUCTION

Leakage plays a crucial role in the behavior of water distribution systems and transmission mains. This fault causes huge water losses (e.g., Ferrante *et al.* 2014b), degradation of water quality (e.g., Fontanazza *et al.* 2015) and important wasteful energy consumption (e.g., Colombo & Karney 2002). These consequences highly affect water companies and their customers worldwide. According to Hyman (1998), 'some of the biggest returns can be made by the supplier reducing the water it wastes'.

The global volume of non-revenue water is estimated to be 346 million cubic meters per day or 126 billion cubic meters per year (Liemberger & Wyatt 2019), and the amount of water lost due to leaks may change depending on countries and transportation systems: from 3–7% in the well-maintained systems (Beuken *et al.* 2008), from 20 to

doi: 10.2166/ws.2021.030

30% in some developing countries and infrequently maintained systems (Lambert 2002). In most drinkable water systems, the problem of aging assets plays a very important role for defining proper strategies towards loss reduction (Beuken *et al.* 2020). In severe cases, water loss may surpass 50% in underdeveloped countries (Van Zyl & Clayton 2007; Puust *et al.* 2010; Zahab *et al.* 2016). In such countries, a successful reduction in water losses may make it possible to increase the population supplied regularly (Schoute & Halim 2010).

Leak detection has attracted the attention of both practitioners and researchers over the last half century. Within the past thirty years, the interest in developing reliable leak detection methodologies has grown considerably. With regard to transmission mains, the performance of transient test-based techniques (TTBTs) is quite encouraging. Within TTBTS, four types of approach have been proposed for the analysis of pressure signals (Colombo *et al.* 2009; Datta & Sarkar 2016; Xu & Karney 2017; Ayati *et al.* 2019): the transient reflection-based method (e.g., Brunone 1999; Liou 1998; Ferrante *et al.* 2014a), the transient damping-based method (Wang *et al.* 2002; Nixon *et al.* 2006; Brunone *et al.* 2019; Capponi *et al.* 2020), the frequency response-based method (e.g., Mpesha *et al.* 2001; Covas *et al.* 2005a; Lee *et al.* 2006; Duan *et al.* 2011; Wang *et al.* 2019; Wang *et al.* 2020), and the inverse transient analysis (ITA), the latter proposed by Liggett & Chen (1994). In particular, for leak detection, ITA has achieved noticeable success by researchers because of its capability to simultaneously detect leak characteristics and calibrate the unknown parameters of the system (e.g., the pressure wave speed). All the unknowns of the problems are determined by optimizing a merit function, which fits the numerically modeled pressure signals to measurements. To this aim, several optimization methods have been applied (Ayati *et al.* 2019). For example, it is worth mentioning the Levenberg–Marquardt method (e.g., Liggett & Chen 1994; Covas & Ramos 2010; Soares *et al.* 2011), genetic algorithms (e.g., Vitkovsky *et al.* 2000; Kim 2005; 2018; Fathi-Moghadam & Kiani 2020), the shuffled complex evolution method (Stephens *et al.* 2004; Lee *et al.* 2005), the model parsimony approach-model error compensation (Vitkovsky *et al.* 2007), the sequential quadratic programming method (e.g., Shamloo & Haghighi 2009), the central force optimization (Haghighi & Ramos 2012), the simulated annealing approach (Huang *et al.* 2015), and the particle swarm optimization, (Ranginkaman *et al.* 2016). A further optimization method, the Nelder–Mead algorithm, has been successfully used for leak detection by Capponi *et al.* (2017) in series with a genetic algorithm in a branched pipe system. This type of algorithm, suitable for multivariable functions, does not imply calculating the derivatives of the objective function. This reduces the computational time and enhances the rapidity of the algorithm compared to other derivative-free methods, as an example genetic algorithms (Pham *et al.* 2011).

ITA procedures have been developed both in the time (e.g., Liggett & Chen 1994; Kapelan *et al.* 2003; Brunone & Ferrante 2004; Covas & Ramos 2010; Haghighi & Ramos 2012) and frequency domains (e.g., Lee *et al.* 2005; Ranginkaman *et al.* 2016; Capponi *et al.* 2017). Moreover, traditionally, fitting is checked by considering a least-square objective function; more recently a matched-filter objective function has been proposed to produce a more robust localization in a noisy environment (Keramat *et al.* 2019). Within leak characterization by means of ITA, one result of all the mentioned methods is better accuracy in terms of leak localization (in many cases a percentage error smaller than the 5%) with respect to leak sizing (an error ranging between 7 and 38%, expressed as the ratio of the leak effective area to the cross-sectional area of the pipes).

In this paper, within a time-domain approach, an ITA-based model is used for leak characterization in a single polymeric pipe by considering pressure signals acquired during laboratory transient tests. The refined model takes into account both the viscoelastic behavior of the pipe material and the unsteady-state friction, with model calibration based on the Nelder–Mead algorithm. In the first stage, the model parameters were determined by considering the experimental pressure signals acquired in an intact pipe. In the second stage, the calibrated ITA solver was used to evaluate leak location and size on the basis of the experimental pressure signals measured in the leaky pipe. With the aim of improving the performance of the calibration procedure and giving an original contribution to this research field, in both stages the objective function has taken into account the pressure traces measured at five sections along the pipe beyond the one at the supply tank.

MATERIAL AND METHODS

Laboratory experiments

Experimental tests were carried out at the Water Engineering Laboratory (WEL) of the University of Perugia, Italy, on a high-density polyethylene pipe (HDPE) with a total length $L = 168.5$ m, an internal diameter $D = 93.3$ mm, and a wall thickness $e = 8.1$ mm (Figure 1). The pipe was supplied by a pressurized tank; during the tests, a pressure head equal to about 20 m was provided by the installed pump. The device simulating the leak (Figure 2) was placed at a distance $L_1 = 63.2$ m downstream of the tank; the effective area of the leak, A_E (=33.6 mm^2), drilled in a steel plate, was evaluated by means of steady-state tests.

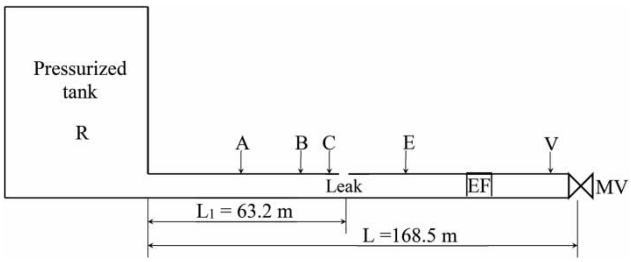

Figure 1 | Laboratory set-up (A, B, C, E, and V = measurement sections; EF = electromagnetic flow meter; MV = maneuver valve).

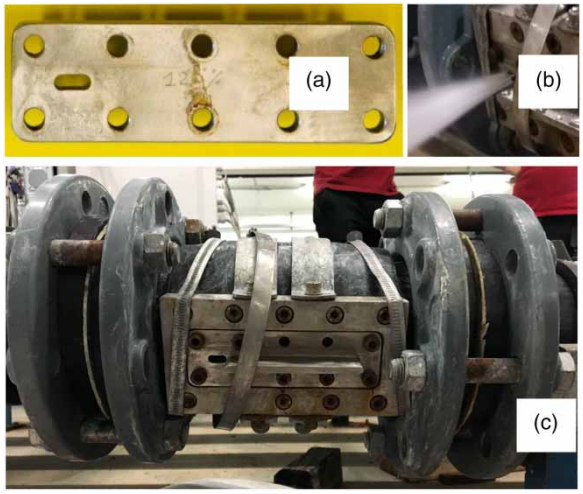

Figure 2 | The device simulating the leak: (a) drilled steel plate, (b) flow through the leak, (c) mounted on the pipe.

Transients were generated by the complete and fast closure of a pneumatically actuated DN50 ball valve, installed at the downstream end section of the pipe.

The pressure signals, H, were measured by means of piezoresistive transducers with a full scale (f.s.) of 3 or 4 bar, depending on the maximum value of the pressure during the transient tests, at the tank R and five measurement sections (Figure 1 and Table 1) with a sampling rate of 2,048 Hz. The measurement uncertainty was rated at ±0.25% of the f.s. The pre-transient discharge downstream of the leak, $Q_{d,0}$, was measured by means of an electromagnetic flow meter (EF in Figure 1), with an uncertainty of the measured discharge of ±0.2% of the measured value. The value of $Q_{d,0}$ was been adjusted by means of a gate valve installed just upstream of the maneuver valve.

The steady-state discharge through the leak, $Q_{L,0}$, was evaluated by means of the well-known Torricelli's (or orifice) equation:

$$Q_{L,0} = A_E\sqrt{2gH_L} \tag{1}$$

by considering the pressure head, H_L, measured at section C (Cassa *et al.* 2010; Ferrante *et al.* 2013, 2014a; Van Zyl 2014; Van Zyl *et al.* 2017; Choura *et al.* 2020).

Three transient tests were carried out in the leaky pipe for different values of $Q_{d,0}$ (= 3.3 L/s, 2.3 L/s, 1.2 L/s) and then of $Q_{L,0}$ (= 0.648 L/s, 0.659 L/s, 0.671 L/s). Values of $Q_{d,0}$ were set for the tests executed, as a reference, in the intact pipe.

In Figures 3 and 4, as an example, the acquired pressure signals were reported for $Q_{d,0} = 3.3$ L/s for the intact and leaky pipes, respectively.

In order to point out the effect of the leak on the transient response of the pipe, in Figure 5, as an example for $Q_{d,0} = 3.3$ L/s, the pressure signal measured at section V is reported for both the intact and leaky pipes. Such pressure traces confirmed that the leak induced additional damping of the pressure peaks as well as the negative pressure

Table 1 | Location of the measurement sections (distances measured from the tank)

Notation	R	A	B	C	E	V
location (m)	0	30.1	54.1	62.6	91.8	166.5

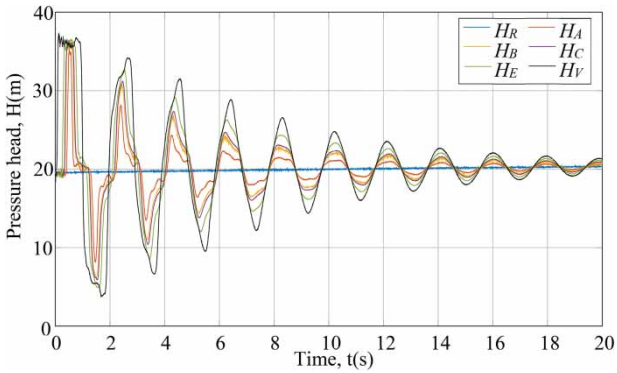

Figure 3 | Experimental pressure signals for $Q_{d,0}$ 3.3 L/s for the intact pipe.

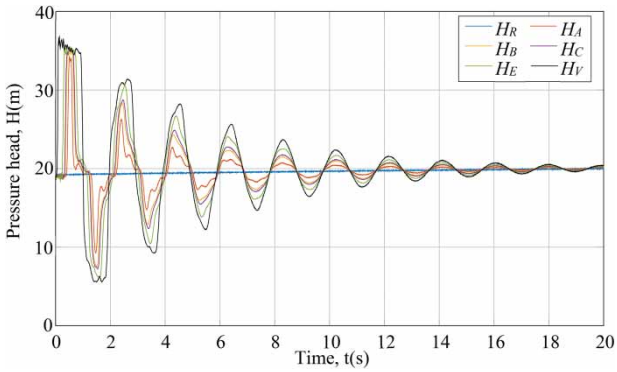

Figure 4 | Experimental pressure signals for $Q_{d,0} = 3.3$ L/s for the leaky pipe.

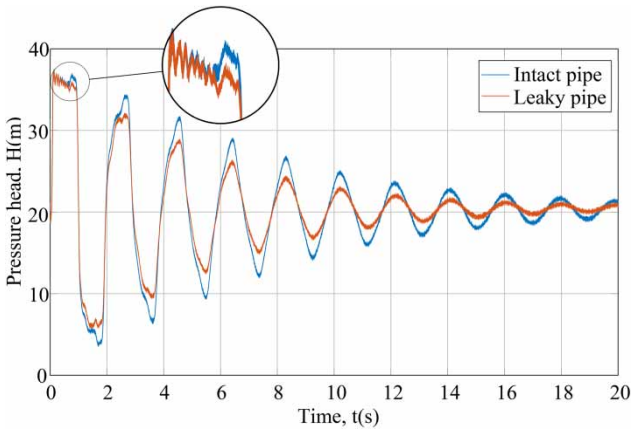

Figure 5 | Experimental pressure signals at measurement section V (just upstream of the maneuver valve) for $Q_{d,0} = 3.3$ L/s and leaky and intact pipes.

waves reflected by the leak in the first pipe characteristic time (the latter highlighted by a circle), on which the transient damping method and the reflected wave method are based, respectively.

Governing equations

According to the literature (Wylie & Streeter 1993; Chaudhry 2014), the governing equations of unsteady flows in pressurized pipe systems are the momentum and continuity equations. Taking into account both unsteady friction and pipe wall viscoelasticity, these equations can be written as:

$$gA\frac{\partial H}{\partial x} + \frac{\partial Q}{\partial t} + h_f = 0 \tag{2}$$

$$\frac{gA}{a^2}\frac{dH}{dt} + \frac{\partial Q}{\partial x} + \frac{2A}{a}\frac{d\varepsilon_r}{dx} = 0 \tag{3}$$

where H = pressure head, Q = discharge, g = gravity acceleration, A = pipe cross-sectional area, h_f = friction term, a = pressure wave speed, ε_r = pipe wall retarded strain, x = space co-ordinate along the pipe axis, and t = time.

The friction term, h_f, is given by the sum of the steady-, h_{fs}, and unsteady-state component, h_{fu}:

$$h_f = h_{fs} + h_{fu} \tag{4}$$

The steady-state component, h_{fs}, was evaluated using the Darcy–Weisbach equation:

$$h_{fs} = \frac{f}{8gD}\frac{Q|Q|}{A^2} \tag{5}$$

where f = friction factor; in the below simulations, as HDPE pipes can be considered as smooth pipes (Brunone & Berni 2010), f has been estimated using the Blasius formula.

The unsteady-state component, h_{fu}, can be evaluated using two types of model (Ghidaoui *et al.* 2005): the instantaneous acceleration-based (IAB) model (Brunone *et al.* 1995; Bergant *et al.* 2001; Brunone & Golia 2008; Pezzinga 2009) and the convolution-based one (Zielke 1968; Trikha 1975; Vardy & Brown 1996; 2010; Meniconi *et al.* 2014). In the executed simulations, h_{fu} was simulated within the IAB approach:

$$h_{fu} = \frac{k_{fu}}{gA}\left(\frac{\partial Q}{\partial t} - aSign(Q)\left|\frac{\partial Q}{\partial x}\right|\right) \tag{6}$$

with the decay coefficient, k_{fu}, given by the Vardy & Brown (1996) formula.

The viscoelastic behavior of the pipe wall is taken into account in Equation (2) by the rate of change in time of the retarded strain, ε_r. In fact, polymeric pipes exhibit an instantaneous-elastic response, ε_e, and a retarded-viscous response, ε_r (Pezzinga *et al.* 2014).

The most popular approach in transient simulation of the behavior of polymeric pipes is the combination of conceptual and mathematical elements, i.e., springs and dashpots. Different combinations of such elements have been reported in the literature (Montgomery & MacKnight 2005): in series (Maxwell models) or in parallel (Kelvin–Voigt (KV) models). In this paper, the generalized KV model (Figure 6), is used where the creep function, $J(t)$, can be written as:

$$J(t) = J_0 + \sum_{i=1}^{n_{KV}} J_i \left(1 - e^{-\frac{t}{\tau_i}}\right) \tag{7}$$

with J_0 = creep compliance of the first spring, n_{KV} = number of the KV elements, J_i = creep compliance (defined as $J_i = 1/E_i$, with E_i = modulus of elasticity) of the of i-th KV element spring, and $\tau_i = \eta_i/E_i$, and η_i are the retardation time and the viscosity of the i-th KV element dashpot, respectively. In order to accurately simulate the viscoelastic behavior of the pipe (Pezzinga *et al.* 2016), in the following numerical investigation, five KV elements were used (i.e., $n_{KV} = 5$), corresponding to 11 viscoelastic parameters to be calibrated.

1-D Numerical model and boundary conditions

The set of partial differential equations, Equations (2) and (3), was been solved using the Method of Characteristics (MOC) (Wylie & Streeter 1993; Chaudhry 2014).

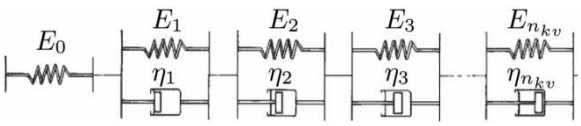

Figure 6 | Generalized Kelvin–Voigt model (from Montgomery & MacKnight 2005).

Regarding the boundary conditions, at the inlet section, according to the characteristics curve of the pump, the pressure at the tank increased slightly with time after the end of the valve complete closure. Consequently, the measured pressure signal at the pressurized tank was assumed as a datum (Meniconi *et al.* 2012); at the leak, Equation (1) was considered. With regard to the maneuver generating the transients, it was assumed to be linear with the closure time, t_c, evaluated experimentally ($t_c = 50$, 40 and 35 milliseconds, for $Q_{d,0} = 3.3$ L/s, 2.3 L/s and 1.2 L/s, respectively). This behavior of t_c vs. $Q_{d,0}$ is justified by the fact that the duration of the maneuver of the pneumatically actuated valve – driven by a compressible fluid pressurized by a constant pressure valve (about 8 bar) – depends on the inertial forces, due to fluid action on the body valve, that increase with $Q_{d,0}$.

The Nelder–Mead optimization method

Within the frequency-domain approach, the Nelder–Mead algorithm has been already used (in series with a genetic algorithm) for the calibration of the viscoelastic parameters (Ferrante & Capponi 2018a, 2018b) and leak detection (Capponi *et al.* 2017) on a branched pipe system. In this paper, the experimental pressure signals acquired in the intact single pipe at six measurement sections were used to calibrate both the viscoelastic parameters and unsteady-state friction coefficient within an ITA procedure based uniquely on the Nelder–Mead algorithm (Nelder & Mead 1965), in the time domain. Successively, the calibrated ITA solver, with the same optimization tool, was utilized to analyze the experimental pressure signals measured in the leaky pipe for leak detection.

The Nelder–Mead algorithm was used for minimizing a nonlinear function F of n variables for unconstrained multidimensional optimization cases. It compared the values of the objective function F at the $(n+1)$ vertices of a general simplex (polygon). Unlike classical gradient methods, the Nelder–Mead algorithm does not imply calculating derivatives. In contrast, it creates a geometric simplex and uses its movement to guide its convergence. At the i-th iteration, the algorithm starts by ordering the vertexes (points generated at the previous iteration) based on the values of the objective function, and determines the best and the worst

vertex (the point with the highest objective function value). Afterwards, it calculates the centroid of the simplex considering all points but the worst and performs a reflection of the latter with respect to the calculated centroid. At this point, the objective function is evaluated and compared to the best vertex. If the objective function value at the new vertex is larger than the latter at the best vertex and smaller than the objective function values at the other vertexes, the reflection vertex substitutes the worst one and the algorithm skips to the evaluation. Otherwise, if it is smaller than the objective function at the best vertex, the algorithm performs an expansion. Again, based on the objective function values of the two vertices (the reflected and expanded), the algorithm selects the best vertex of these two (i.e., the one with the minimum value of the objective function), affects its value to the worst vertex and skips to the evaluation. If objective function value at the reflected vertex is larger than the latter at the other points, the algorithm proceeds to contraction (Lagarias *et al.* 1998). Based on a comparison between the objective function values at the reflected vertex and the worst vertex, the algorithm decides which type of contraction, between the worst vertex and the centroid, to follow. If the reflected value is larger than the worst vertex, the algorithm chooses an inside contraction, otherwise, it chooses an outside contraction. Eventually, it evaluates the objective function value of the contracted vertex and compares it to the worst and reflected vertex. If the new solution is minimal, it substitutes the worst vertex with the contracted vertex, otherwise it performs a shrinkage around the best vertex. In other words, the function values at each vertex are evaluated iteratively, and the worst vertex with the largest function value is replaced by a new vertex. Otherwise, a simplex will be shrunk around the best vertex, and this process will be continued until a desired minimum is met or no further improvement of the objective function are achieved. In order to minimize properly function F, four scalar parameters must be specified as an input: the coefficients of reflection, ρ, expansion, χ, contraction, γ, and shrinkage, σ; in this paper the following values were into account: $\rho = 1$, $\chi = 2$, $\gamma = 0.5$, and $\sigma = 0.5$.

For the sake of clarity, some comments are reported below about the role of constraints and boundary conditions within the used optimization procedure.

As mentioned, the Nelder–Mead optimization algorithm, implemented in MATLAB©, was used for unconstrained optimization problems. However, some constraints can be introduced by properly defining the objective function and/or setting some options for the optimization in the used code. Therefore, this type of constraints concerns only the decision variables. With regard to the boundary conditions, they were defined properly and preserved regardless of the optimization process. Moreover, there were constraints on the decision variables – the leak size must be non-negative and the location ratio must range between 0 and 1 – that can be taken into account reliably in the code. In fact, a negative value of the leak size would cause a positive reflected pressure wave that is the contrary of the leak transient response (i.e., a negative reflected pressure wave). This difference increases the error in the optimization procedure. Mathematically speaking, the curve of the leak size vs. the error would take the shape of a parabola of a directrix parallel to the leak size axis and a focus somewhere in the interval (the real value $\pm$ a small variation). This would guide the optimization process towards a value in the right interval. For this reason, there was no need for a constraint on the leak size (if this parameter leaves the interval, the object function value will increase and this disagrees with the fact that the problem is a minimization one). Regarding the leak location ratio, this parameter must be in the interval [0, 1], equivalent to [0, 100%] of the total length (0% – at the reservoir, 100% – at the valve). For any value outside such a range, the code will not run. In fact, the algorithm relies on testing a flawed section of the pipe as if it is a junction of pipes with a default. In MOC, sections are numbered from 1 to $N + 1$. If the flawed section is 1 or $N + 1$, the code will not run as no pipe junction exists. Starting from 2 to N, the algorithm splits the pipe into two pipes with a flawed junction at any section (for example, if the flawed section is 1, i.e., the leak is at the reservoir, the first part of the pipe would be of zero length whereas the second would have a length equal to L. For this case, and similarly for the $N + 1$ section, the algorithm gives an error). For this reason, the code has been written inside a try-catch loop.

Within the used calibration procedure, the mean squared error (MSE) was assumed as the objective function F to minimize. In terms of pressure head, H, it can be

written:

$$MSE = \frac{1}{N_t \times N_p} \sum_t \sum_p (H_p^m(t) - H_p^s(t))^2 \quad (8)$$

where the superscripts 's' and 'm' indicate the simulated and measured values, respectively, p = location (i.e., the measurement sections V, E, C, B and A), N_p = number of the measurement sections, and N_t ($= \Delta T/\Delta t$) is the number of the considered instances of time, ΔT = sample length of the pressure signals, Δt ($= \Delta x/a$) is the MOC time-step, and Δx = space-step.

Even if it is obvious, for the sake of completeness, it needs to be pointed out that, as it will be discussed below, the accuracy and computational expense of the proposed ITA procedure is a result not only of the used Nelder–Mead optimization algorithm, but also of the characteristics of the model simulating the transient response of the system, particularly the temporal and spatial discretization criteria within MOC, the sample length of the pressure signals, the pipe material behavior and the unsteady-state energy dissipation mechanisms.

MODEL CALIBRATION

As mentioned, the model calibration procedure was based on the pressure signals acquired during transient tests executed in the intact pipe. Particularly, within the KV parameters calibration, three different approaches have been followed: (i) k_{fu} is assumed as a further parameter to be calibrated; (ii) k_{fu} is evaluated by the Vardy & Brown (1996) formula; and (iii) the unsteady friction is neglected ($k_{fu} = 0$). The sample length of the pressure signals, ΔT, used for the calibration was set equal to 20 s as in this time interval the pressure waves generated during the executed transients dissipate significantly in the considered tank–pipe–valve system (Figure 3). Moreover, the MOC spatial discretization was fixed to $N = 100$ pipe elements, with $\Delta x = 1.68$ m. Finally, the values obtained by Covas *et al.* (2004, 2005b) were assumed as initial guess values of the KV parameters.

Calibration of the KV parameters and k_{fu}

The results of the calibration reported in Table 2 show quite close values of the KV parameters irrespective from the value of $Q_{d,0}$. In this table, the symbol '-' indicates that the values of the retardation time and the corresponding creep compliance of the i-th KV element have been disregarded. This happens when the retardation time, τ_i, exceeds the length of the sample time, which means that ΔT is assumed as the maximum of the retardation time.

The Nelder–Mead algorithm (1965) was successful in the calibration of the creep parameters in terms of the resulting MSE and time and computational efficiency. The differences between the results of the calibrations executed considering the three tests on the intact pipe can be due to the fact that the derivative-free optimization methods are stochastic in determining the minimum and capable only of delimiting

Table 2 | Calibration results when the unsteady-state coefficient as a parameter

	Calibrated parameters: J_i (10^{-10} Pa), τ_i (s)							
Discharge $Q_{d,0}$ (L/s)		$i = 0$	$i = 1$	$i = 2$	$i = 3$	$i = 4$	$i = 5$	***MSE*** **(m²)**
3.3	J_i	6.284	0.811	0.091	0.000[a]	0.836	0.766	0.077
	τ_i		0.128	0.189	1.054	1.328	2.479	
	k_{fu}	0.0442						
2.3	J_i	6.416	0.839	0.018	0.793	3.766	1.014	0.043
	τ_i		0.125	0.638	1.127	7.456	13.205	
	k_{fu}	0.0129						
1.2	J_i	6.294	0.708	0.657	0.032	–	–	0.012
	τ_i		0.120	0.574	0.768	–	–	
	k_{fu}	0.0536						

[a] $J_3 = 1.614 \times 10^{-16}$ Pa.

the closest local minima to the suggested initial guess, *IG*. Moreover, such differences can also be a natural effect of the conceptual nature of the KV model (Covas *et al.* 2004; Weinerowska-Bords 2007; Pezzinga *et al.* 2016). As a consequence, the same result (i.e., the same pressure signal) can be obtained by assuming different values of the KV parameters. In other words, from a mathematical point of view, several combinations of the decision variables (i.e., the KV parameters and k_{fu}) correspond to almost the same value of the objective function. Finally, the fact that *MSE* decreases with $Q_{d,0}$ is reasonable since the larger $Q_{d,0}$, the larger the generated pressure waves and then the more reliable the ITA.

Calibration of the KV parameters with a calculated k_{fu}

At this stage, the calibration process includes only the KV parameters (i.e., J_i and τ_i) whereas k_{fu} has been incorporated into the model as a calculated variable by the Vardy & Brown (1996) equation. The calibration process outcome is summarized in Table 3. With respect to the approach where both KV parameters and k_{fu} were calibrated, it can be noted that in this approach *MSE* slightly increases.

Calibration of the KV parameters with $k_{fu} = 0$

Within the third approach, the KV parameters are assumed as a decision variable whereas the unsteady-state friction is neglected ($k_{fu} = 0$). The results of such a calibration procedure are shown in Table 4 and in Figure 7, where, as an example for $Q_{d,0} = 1.2$ L/s, the calibrated pressure signals at the measurement sections along the pipe are compared with the experimental ones. The very good performance of the model when unsteady-state friction is neglected – the experimental and calibrated pressure signals are almost indistinguishable – confirms the negligible relevance of h_{fu} in polymeric pipes pointed out in Duan *et al.* (2010).

Table 3 | Calibration results with k_{fu} calculated

		Calibrated parameters: J_i (10^{-10} Pa), τ_i (s)						
Discharge $Q_{d,0}$ (L/s)		**$i = 0$**	**$i = 1$**	**$i = 2$**	**$i = 3$**	**$i = 4$**	**$i = 5$**	***MSE* (m²)**
3.3	J_i	6.200	0.764	0.081	0.716	0.000[a]	0.592	0.082
	τ_i		0.117	0.162	1.031	2.594	3.518	
2.3	J_i	6.233	0.779	0.337	0.063	0.987	2.341	0.053
	τ_i		0.125	0.647	0.911	10.263	13.085	
1.2	J_i	6.168	0.814	0.270	0.039	0.000[b]	–	0.015
	τ_i		0.139	0.759	1.091	6.395	–	

[a] $J_4 = 0.904 \times 10^{-16}$ Pa.
[b] $J_4 = 0.494 \times 10^{-15}$ Pa.

Table 4 | Calibration results when the unsteady-state friction is neglected ($k_{fu} = 0$)

		Calibrated parameters: J_i (10^{-10} Pa), τ_i (s)						
Discharge $Q_{d,0}$ (L/s)		**$i = 0$**	**$i = 1$**	**$i = 2$**	**$i = 3$**	**$i = 4$**	**$i = 5$**	***MSE* (m²)**
3.3	J_i	6.382	0.746	0.078	0.989	0.000[a]	0.994	0.080
	τ_i		0.115	0.160	0.794	2.837	2.855	
2.3	J_i	6.438	0.811	0.018	0.684	3.907	0.941	0.039
	τ_i		0.118	0.646	0.834	6.247	13.562	
1.2	J_i	5.411	1.157	0.000[b]	1.274	0.084	–	0.005
	τ_i		0.007	0.100	0.297	1.399	–	

[a] $J_4 = 1.273 \times 10^{-16}$ Pa.
[b] $J_2 = 0.645 \times 10^{-15}$ Pa.

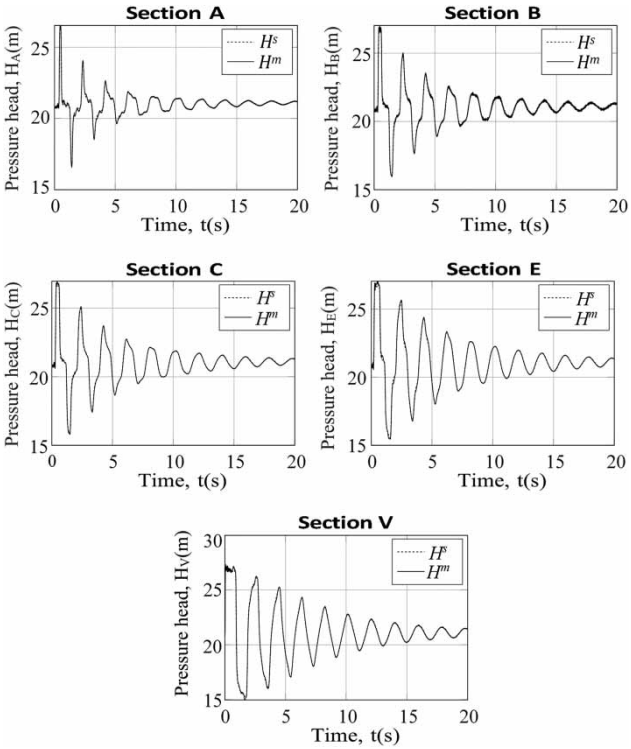

Figure 7 | Experimental (subscript 'm') versus calibrated (subscript 's'), with $k_{fu} = 0$, pressure signals at the measurement sections along the intact pipe for $Q_{d,0} = 1.2$ L/s.

According to the KV approach, the pressure wave speed, a, depends on the value of the creep compliance of the first spring, J_0, through the one of the Young modulus of elasticity. As a consequence, different values of J_0, resulting from different methods of calibration, imply different values of a. It is worth pointing out that within the above calibration procedures the value of a did not change significantly and no clear trend of a with a given calibration procedure was identified. The obtained values of a, ranging from 368.9 m/s to 399.9 m/s, were compatible not only with the mechanical characteristics of the installed pipes but also with the measured travel times of the pressure waves.

LEAK LOCATION AND SIZING

As for the procedure followed for the calibration of the viscoelastic parameters and unsteady-state friction coefficient, in the ITA procedure for leak characterization, the leak size and location were calibrated by minimizing the MSE given by Equation (8). Moreover, the performance of the algorithm was evaluated by means of the relative mean errors:

$$\varepsilon_L = \left| \frac{L_1^S - L_1}{L_1} \right| \times 100 \tag{9a}$$

$$\varepsilon_S = \left| \frac{A_E^S - A_E}{A_E} \right| \times 100 \tag{9b}$$

with the subscripts L and s indicating the leak location and size, respectively. Within such an ITA procedure, for accuracy enhancement purposes, the number of pipe elements doubled ($N = 200$), with $\Delta x = 0.84$ m.

In the below subsections, the role of the initial guesses, length of the sampling time, and considered measurement sections is examined, as factors influencing the performance of the proposed procedure.

The role of the initial guesses, *IG*

As a preliminary step, a series of direct simulations was executed by means of MOC for evaluating MSE as a two-variables function of the leak location and size, within the intervals 0%L–100%L and 0–100 mm^2, respectively. In the carried-out simulations, the steps were 0.1% for the leak dimensionless location and 0.1 mm^2 for its size. As an example, the case of $Q_{d,0} = 3.3$ L/s with k_{fu} calculated is discussed below. As a result of the numerical simulations, the values associated with the global minimum of *MSE* (indicated by the square in Figure 8) were ${L_1}^s = 64.87$ m and $A_E^s = 34.7$ mm^2. The associated relative errors with respect to the exact values (a cross in Figure 8) were $\varepsilon_L = 0.78\%$ and $\varepsilon_S = 3.27\%$, respectively. Such values, i.e., the global minimum and the exact ones, allow an estimation of the performance of the ITA procedure based on the Nelder–Mead algorithm.

Because of the mentioned sensitivity of the results to initial guesses, several *IG* for leak location have been considered, whereas for leak size it was assumed that $IG = 0$.

In the ITA procedure, firstly, the pipe length was divided into 11 equidistant nodes and the algorithm evaluates *MSE* for all nodes. Then, the two nodes with the lowest *MSE* values were selected, the in-between value is chosen and the optimization procedure for the leak parameters

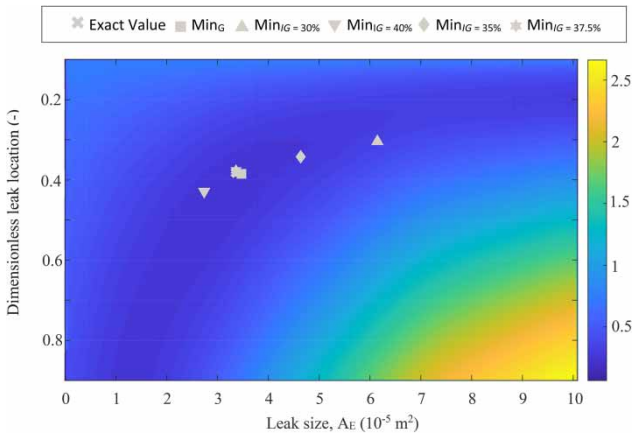

Figure 8 | MSE vs. leak location and size for $Q_{d,0} = 3.3$ L/s, $\Delta T = 20$ s, with all the pressure signals considered and k_{fu} calculated: direct transient simulations and Nelder–Mead algorithm-based ITA.

estimation restarts. In Figure 8, the up-pointing triangle symbol corresponds to the local minima of *MSE* given by the optimization algorithm for $IG = 30\%$ ($MSE = 0.32$). In the same figure, the down-pointing triangle symbol indicates the local minima for $IG = 40\%$ (MSE = 0.31). The relative mean errors associated with $IG = 30\%$ (40%) for the leak location and size are $\varepsilon_L = 20.3\%$ (12.8%) and $\varepsilon_s = 82.85\%$ (18.59%) that correspond to $L_1{}^s = 50.7$ m (71.4 m) and $A_E^s = 61.44$ mm^2 (27.35 mm^2), respectively. Then, for $IG =$ 35%, it results $MSE = 0.30$ with the relative errors $\varepsilon_L =$ 10.34% for leak location and $\varepsilon_s = 37.87\%$ for leak size, corresponding to $L_1{}^s = 57.01$ m and $A_E^s = 46.32$ mm^2, respectively (diamond symbol in Figure 8). These results, that will be confirmed also by the below simulations, indicated that the performance of the proposed ITA procedure in terms of leak sizing is generally worse than the one in terms of leak location.

The role of the length of the sampling time, ΔT

To analyze the relevance of ΔT, four sample time lengths were considered (ΔT = 20, 10, 5 and 2 s). For $Q_{d,0} = 3.3$ L/s, $IG = 35\%$, and with k_{fu} assumed as a parameter in the calibration, the results (Table 5) point out the crucial role of ΔT. Precisely, the smaller the ΔT, the smaller the ε_L. This behavior is due to the fact that the effect of the leak location on the pressure signals is very visible in the first characteristic period. In contrast, the smaller the ΔT, the larger the ε_S, as

Table 5 | The role of the length of the sample time on the leak parameters estimation accuracy (for $Q_{d,0} = 3.3$ L/s, and $IG = 35\%$, with all the pressure signals considered and k_{fu} calibrated)

ΔT (s)	2	5	10	20
ε_S (%)	38.10	38.09	37.93	22.00
ε_L (%)	0.49	0.49	0.49	3.40
MSE (m^2)	0.61	0.71	0.54	0.29

the important effect of the leak size on the damping of pressure peaks (Capponi *et al.* 2020). Moreover, these simulations confirm that ε_S is significantly larger that ε_L.

The role of the considered measurement sections

Because of the poor accessibility of pipe systems, particularly transmission mains, it is of interest to analyze the effect of the number and location of the measurement sections on the accuracy in the leak parameters estimation. The results of the executed numerical simulations in which different measurement sections were considered (Table 6) point out that, when a single section is taken into account, the closer the measurement section to the transient source the better the results of the ITA procedure for leak location. Such a behavior confirms the results reported in Wang (2021). Moreover, the use of a combination of

Table 6 | The role of the measurement sections number and location on the accuracy of leak characterization ($Q_{d,0} = 3.3$ L/s, $\Delta T = 20$ s, and $IG = 35\%$, with k_{fu} calibrated)

Number of sections	Notation	ε_L (%)	ε_S (%)
1	A[a]	3.89	46.20
	B[a]	3.50	18.68
	C[a]	3.40	44.95
	E[b]	3.40	23.67
	V[b]	0.02	27.06
2	(E, V)[b]	3.40	21.41
	(C, E)[c]	3.40	23.76
	(B, C)[a]	3.40	21.41
3	(C, E, V)	3.40	21.41
	(A, B, C)[a]	5.34	35.75
	(A, C, V)	3.40	20.21
5	All	3.40	22.00

[a]Section between the tank and the leak.
[b]Section between the leak and the maneuver valve.
[c]Section close to the leak.

measurement sections (i.e., two, three or the five sections upstream or downstream of the leak the leak or close to the transient source) do not give rise to any enhancement in locating the leak (Table 6), but it improves the leak sizing. This result, quite different with respect to Wang's outcomes, merits further analysis by considering different pipe materials and system layouts. As for the above numerical experiments, values reported in Table 6 point out that $\varepsilon_S \gg \varepsilon_L$.

CONCLUSIONS

An ITA procedure for model calibration in a polymeric pipe test facility at the WEL of the University of Perugia is presented. A five-elements generalized KV model was chosen to characterize the pipe wall behavior during transients. The Nelder–Mead algorithm was used for minimization of the chosen objective function for three values of the discharge. The proposed calibration procedure allowed estimation of 11 viscoelastic parameters and the unsteady-state friction decay coefficient by considering pressure signals acquired at six measurement sections in an intact pipe. Successively, the calibrated model was used for leak detection (location and size) on the basis of the pressure signals measured in a leaky pipe. The role of the initial guesses, length of the sample period and characteristics of the considered measurement sections on the accuracy of the procedure were investigated.

As shown, the proposed ITA procedure was successful in localizing the leak with acceptable accuracy; in contrast, as found for most of the procedures available in the literature, the performance in terms of leak sizing was quite worse. The analysis of this different behavior for the ITA procedure in terms of leak location with respect to leak sizing merits more in-depth analysis with further numerical and experimental tests. As preliminary working hypotheses, the ambiguity of some features of the pressure signal as a mark of a given leak at a given location, pointed out in Brunone *et al.* (2019) and Capponi *et al.* (2020), and the role of the pipe material, as conjectured in Meniconi *et al.* (2013), could be considered as possible causes of the poor performance in leak sizing. In contrast, the good match between simulated and real leak location depends on the fact that this sort of feature is obtained based on the travel time of the pressure wave reflected by the leak, that is quite easy to capture.

ACKNOWLEDGEMENTS

This research has been partially funded by the Hong Kong (HK) Research Grant Council Theme-Based Research Scheme and the HK University of Science and Technology (HKUST) under the project 'Smart Urban Water Supply System (Smart UWSS)'.

DATA AVAILABILITY STATEMENT

All relevant data are included in the paper or its Supplementary Information.

REFERENCES

Ayati, A. H., Haghighi, A. & Lee, P. 2019 Statistical review of major standpoints in hydraulic transient-based leak detection. *Journal of Hydraulic Structures* **5** (1), 1–26.

Bergant, A., Simpson, A. R. & Vitkovsky, J. 2001 Developments in unsteady pipe flow friction modelling. *Journal of Hydraulic Research* **39** (3), 249–257.

Beuken, R. H. S., Lavooij, C. S. W., Bosch, A. & Schaap, P. G. 2008 Low leakage in the Netherlands confirmed. *Eighth Annual Water Distribution Systems Analysis Symposium (WDSA)* **2006**. doi: 10.1061/40941(247)174.

Beuken, R., Eijkman, J., Savic, D., Hummelen, A. & Blokker, M. 2020 Twenty years of asset management research for Dutch drinking water utilities. *Water Supply* **20** (8), 2941–2950. doi:10.2166/ws.2020.179.

Brunone, B. 1999 Transient test-based technique for leak detection in outfall pipes. *Journal of Water Resources Planning and Management* **125** (5), 302–306.

Brunone, B. & Berni, A. 2010 Wall shear stress in transient turbulent pipe flow by local velocity measurement. *Journal of Hydraulic Engineering* **136** (10), 716–726.

Brunone, B. & Ferrante, M. 2004 Pressure waves as a tool for leak detection. *Urban Water Journal* **1** (2), 145–155.

Brunone, B. & Golia, U. M. 2008 Discussion of 'Systematic evaluation of one-dimensional unsteady friction models in simple pipelines' by J.P. Vitkovsky, A. Bergant, A.R. Simpson, and M. F. Lambert. *Journal of Hydraulic Engineering* **134** (2), 282–284.

Brunone, B., Golia, U. M. & Greco, M. 1995 The effects of two-dimensionality on pipe transients modeling. *Journal of Hydraulic Engineering* **121** (12), 906–912.

Brunone, B., Meniconi, S. & Capponi, C. 2019 Numerical analysis of the transient pressure damping in a single polymeric pipe with a leak. *Urban Water Journal* **15**, 760–768.

Capponi, C., Ferrante, M., Zecchin, A. C. & Gong, J. 2017 Leak detection in a branched system by inverse transient analysis with the admittance matrix method. *Water Resources Management* **31**, 4075–4089.

Capponi, C., Meniconi, S., Lee, P. J., Brunone, B. & Cifrodelli, M. 2020 Time-domain analysis of laboratory experiments on the transient pressure damping in a leaky polymeric pipe. *Water Resources Management* **34**, 501–514.

Cassa, A. M., van Zyl, J. E. & Laubscher, R. F. 2010 A numerical investigation into the effect of pressure on holes and cracks in water supply pipes. *Urban Water Journal* **7** (2), 109–120.

Chaudhry, M. H. 2014 *Applied Hydraulic Transients*. Springer, New York.

Choura, O., Elaoud, S. & Brunone, B. 2020 Transient flow study and fault detection in polymeric pipelines inverse-transient-based leak detection algorithm. In: *Design and Modeling of Mechanical Systems IV* (N. Aifaoui, Z. Affi, M. S. Abbes, L. Walha, M. Haddar, L. Romdhane, A. Benamara, M. Chouchane & F. Chaari, eds). CMSM 2019 – March 18–20, Hammamet, Tunisia. Lecture Notes in Mechanical Engineering. Springer, Cham. doi:10.1007/978-3-030-27146-6_14.

Colombo, A. F. & Karney, B. W. 2002 Energy and costs of leaky pipes: toward comprehensive picture. *Journal of Water Resources Planning and Management* **128** (6), 441–450.

Colombo, A., Lee, P. & Karney, B. W. 2009 A selective literature review of transient-based leak detection methods. *Journal of Hydro-Environment Research* **2**, 212–227.

Covas, D. & Ramos, H. 2010 Case studies of leak detection and location in water pipe systems by inverse transient analysis. *Journal of Water Resources Planning and Management* **136** (2), 248–257.

Covas, D., Stoianov, I., Ramos, H., Graham, N. & Maksimovic, C. 2004 The dynamic effect of pipe-wall viscoelasticity in hydraulic transients. Part I: experimental analysis and creep characterization. *Journal of Hydraulic Research* **42**, 517–532.

Covas, D., Ramos, H. & De Almeida, A. B. 2005a Standing wave difference method for leak detection in pipeline systems. *Journal of Hydraulic Engineering* **131**, 1106–1116.

Covas, D., Stoianov, I., Mano, J. F., Ramos, H., Graham, N. & Maksimovic, C. 2005b The dynamic effect of pipe-wall viscoelasticity in hydraulic transients. Part II: model development, calibration and verification. *Journal of Hydraulic Research* **43**, 56–70.

Datta, S. & Sarkar, S. 2016 A review on different pipeline fault detection methods. *Journal of Loss Prevention in the Process Industries* **41**, 97–106.

Duan, H. F., Ghidaoui, M., Lee, P. J. & Tung, Y.-K. 2010 Unsteady friction and viscoelasticity in pipe fluid transients. *Journal of Hydraulic Research* **48**, 354–362.

Duan, H. F., Lee, P. J., Ghidaoui, M. S. & Tung, Y. K. 2011 Leak detection in complex series pipelines by using the frequency response method. *Journal of Hydraulic Research* **49** (2), 213–221.

Fathi-Moghadam, M. & Kiani, S. 2020 Simulation of transient flow in viscoelastic pipe networks. *Journal of Hydraulic Research* **58** (3), 531–540.

Ferrante, M. & Capponi, C. 2018a Calibration of viscoelastic parameters by means of transients in a branched water pipeline system. *Urban Water Journal* **15**, 9–15.

Ferrante, M. & Capponi, C. 2018b Comparison of viscoelastic models with a different number of parameters for transient simulations. *Journal of Hydroinformatics* **20**, 18–33.

Ferrante, M., Massari, C., Brunone, B. & Meniconi, S. 2013 Leak behaviour in pressurized PVC pipes. *Water Science & Technology: Water Supply* **13** (4), 987–992.

Ferrante, M., Brunone, B., Meniconi, S., Karney, B. W. & Massari, C. 2014a Leak size, detectability and test conditions in pressurized pipe systems. *Water Resources Management* **28**, 4583–4598.

Ferrante, M., Meniconi, S. & Brunone, B. 2014b Local and global leak laws. *Water Resources Management* **28**, 3761–3782.

Fontanazza, C. M., Notaro, V., Puleo, V., Nicolosi, P. & Freni, G. 2015 Contaminant intrusion through leaks in water distribution system: experimental analysis. *Procedia Engineering* **119**, 426–433.

Ghidaoui, M. S., Zhao, M., McInnis, D. A. & Axworthy, D. H. 2005 A review of water hammer theory and practice. *Applied Mechanics Reviews* **58**, 49–76.

Haghighi, A. & Ramos, H. M. 2012 Detection of leakage freshwater and friction factor calibration in drinking networks using central force optimization. *Water Resources Management* **26** (8), 2347–2363.

Huang, Y.-C., Lin, C.-C. & Yeh, H.-D. 2015 An optimization approach to leak detection in pipe networks using simulated annealing. *Water Resources Management* **29** (11), 4185–4201.

Hyman, L. S. 1998 *The Water Business: Understanding the Water Supply and Wastewater Industry*. Public Utility Reports, Vienna, VA.

Kapelan, Z. S., Savic, D. A. & Walters, G. A. 2003 A hybrid inverse transient model for leakage detection and roughness calibration in pipe networks. *Journal of Hydraulic Research* **41**, 481–492.

Keramat, A., Wang, X., Louati, M., Meniconi, S., Brunone, B. & Ghidaoui, M. S. 2019 Objective functions for transient-based pipeline leakage detection in a noisy environment: least square and matched-filter. *Journal of Water Resources Planning and Management* **145** (10), 04019042.

Kim, S. H. 2005 Extensive development of leak detection algorithm by impulse response method. *Journal of Hydraulic Engineering* **131**, 201208.

Kim, S. H. 2018 Development of multiple leakage detection method for a reservoir pipeline valve system. *Water Resources Management* **32** (6), 2099–2112.

Lagarias, J. C., Reeds, J. A., Wright, M. H. & Wright, P. E. 1998 Convergence properties of the Nelder–Mead simplex method in low dimensions. *SIAM Journal on Optimization* **9**, 112147.

Lambert, A. O. 2002 International report: water losses management and techniques. *Water Science and Technology: Water Supply* **2**, 1–20.

Lee, P. J., Vitkovsky, J. P., Lambert, M. F., Simpson, A. R. & Ligget, J. A. 2005 Frequency domain analysis for detecting pipeline leaks. *Journal of Hydraulic Engineering* **131** (7), 596–604.

Lee, P. J., Lambert, M. F., Simpson, A. R., Vitkovsky, J. P. & Ligget, J. A. 2006 Experimental verification of the frequency response method for pipeline leak detection. *Journal of Hydraulic Research* **44** (5), 693–707.

Liemberger, R. & Wyatt, A. 2019 Quantifying the global non-revenue water problem. *Water Supply* **19** (3), 831–837.

Liggett, J. A. & Chen, L. C. 1994 Inverse transient analysis in pipe networks. *Journal of Hydraulic Engineering* **120**, 934–955.

Liou, C. P. 1998 Pipeline leak detection by impulse response extraction. *Journal of Fluids Engineering* **120**, 833–838.

Meniconi, S., Brunone, B., Ferrante, M. & Massari, C. 2012 Transient hydrodynamics of in-line valves in viscoelastic pressurized pipes: long-period analysis. *Experiments in Fluids* **53**, 265–275.

Meniconi, S., Duan, H.-F., Lee, P. J., Brunone, B., Ghidaoui, M. & Ferrante, M. 2013 Experimental investigation of coupled frequency- and time-domain transient test-based techniques for partial blockage detection in pipelines. *Journal of Hydraulic Engineering* **139** (10), 1033–1040.

Meniconi, S., Duan, H. F., Brunone, B., Ghidaoui, M. S., Lee, P. J. & Ferrante, M. 2014 Further developments in rapidly decelerating turbulent pipe flow modeling. *Journal of Hydraulic Engineering* **140** (7), 04014028.

Montgomery, T. & MacKnight, W. 2005 *Introduction to Polymer Viscoelasticity (Third Edition)*. John Wiley and Sons, New Jersey, USA.

Mpesha, W., Gassman, S. L. & Chaudhry, M. H. 2001 Leak detection in pipes by frequency response method. *J. Hydraul. Eng.* **127** (2), 134–147.

Nelder, J. A. & Mead, R. 1965 A simplex method for function minimization. *The Computer Journal* **7**, 308–313.

Nixon, W., Ghidaoui, M. S. & Kolyshkin, A. A. 2006 Range of validity of the transient damping leakage detection method. *Journal of Hydraulic Engineering* **132** (9), 944–957.

Pezzinga, G. 2009 Local balance unsteady friction model. *Journal of Hydraulic Engineering* **135** (1), 45–56.

Pezzinga, G., Brunone, B., Cannizzaro, D., Ferrante, M., Meniconi, S. & Berni, A. 2014 Two-dimensional features of viscoelastic models of pipe transients. *Journal of Hydraulic Engineering* **140** (8), 0401403.

Pezzinga, G., Brunone, B. & Meniconi, S. 2016 Relevance of pipe period on Kelvin–Voigt viscoelastic parameters: 1D and 2D inverse transient analysis. *Journal of Hydraulic Engineering* **142** (12), 04016063.

Pham, N., Malinowski, A. & Bartczak, T. 2011 Comparative study of derivative free optimization algorithms. *IEEE Transactions on Industrial Informatics* **7** (4), 592–600.

Puust, R., Kapelan, Z., Savic, D. A. & Koppel, T. 2010 A review of methods for leakage management in pipe networks. *Urban Water Journal* **7**, 25–45.

Ranginkaman, M. H., Haghighi, A. & Vali Samani, H. M. 2016 Inverse frequency response analysis for pipelines leak detection using the particle swarm optimization. *International Journal of Optimization in Civil Engineering* **6** (1), 1–12.

Schoute, M. & Halim, R. D. 2010 Resolving strategy paradoxes of water loss reduction: a synthesis in Jakarta. *Resources, Conservation and Recycling* **54**, 1322–1330.

Shamloo, H. & Haghighi, A. 2009 Leak detection in pipelines by inverse backward transient analysis. *Journal of Hydraulic Research* **47** (3), 311–318.

Soares, A. K., Covas, D. I. C. & Reis, L. F. R. 2011 Leak detection by inverse transient analysis in an experimental PVC pipe system. *Journal of Hydroinformatics* **13**, 153–166.

Stephens, M., Lambert, M., Simpson, A., Vitkovsky, J. & Nixon, J. 2004 Field tests for discrete blockage, air pocket and leak detection using inverse transient analysis in water distribution pipes. *Sixth Annual Symposium on Water Distribution Systems Analysis, ASCE* **27** (1), 1–10.

Trikha, A. K. 1975 An efficient method for simulating frequency-dependent friction in transient liquid flow. *Journal of Fluids Engineering* **97** (1), 97–105.

Van Zyl, J. E. 2014 Theoretical modeling of pressure and leakage in water distribution systems. *Procedia Engineering* **89**, 273–277.

Van Zyl, J. E. & Clayton, C. R. I. 2007 The effect of pressure on leakage in water distribution systems. *Proceedings of the Institution of Civil Engineers – Water Management* **160**, 109–114.

Van Zyl, J. E., Lambert, A. O. & Collins, R. 2017 Realistic modeling of leakage and intrusion flows through leak openings in pipes. *Journal of Hydraulic Engineering* **143** (9), 04017030.

Vardy, A. E. & Brown, J. M. B. 1996 On turbulent, unsteady, smooth-pipe friction. 7th International Conference on Pressure Surges and Fluid Transients in Pipelines and Open Channels, BHR Group, 16–18 April 1996, Harrogate, UK, pp. 289–311.

Vardy, A. E. & Brown, J. M. B. 2010 Evaluation of unsteady wall shear stress by Zielke's method. *Journal of Hydraulic Engineering* **136** (7), 453–456.

Vitkovsky, J. P., Simpson, A. R. & Lambert, M. F. 2000 Leak detection and calibration using transients and genetic algorithms. *Journal of Water Resources Planning and Management* **126**, 262–265.

Vitkovsky, J. P., Lambert, M. F., Simpson, A. R. & Ligget, J. A. 2007 Experimental observation and analysis of inverse transients for pipeline leak detection. *Journal of Water Resources Planning and Management* **133** (6), 519–530.

Wang, X. 2021 Uniformly optimal multi-sensor design in pipe networks for transient-based leakage localization. *Mechanical Systems and Signal Processing* **149**, 107216.

Wang, X.-J., Lambert, M. F., Simpson, A. R., Liggett, J. A. & Vitkovsky, J. P. 2002 Leak detection in pipelines using the damping of fluid transients. *Journal of Hydraulic Engineering* **128** (7), 697–711.

Wang, X., Palomar, D. P., Zhao, L., Ghidaoui, M. S. & Murch, R. D. 2019 Spectral-based methods for pipeline leakage localization. *Journal of Hydraulic Engineering* **145** (3), 04018089.

Wang, X., Waqar, M., Yan, H.-C., Louati, M., Ghidaoui, M. S., Lee, P. J., Meniconi, S., Brunone, B. & Karney, B. 2020 Pipeline leak localization using matched-field processing incorporating prior information of modeling error. *Mechanical Systems and Signal Processing* **143**, 106849.

Weinerowska-Bords, K. 2007 Accuracy and parameter estimation of elastic and viscoelastic models of the water hammer. *Task Quarterly* **11**, 383–395.

Wylie, E. & Streeter, V. 1993 *Fluid Transients in Systems*. Prentice-Hall Inc., Englewood Cliffs, NJ, USA.

Xu, X. & Karney, B. 2017 An overview of transient fault detection techniques. In: *Modeling and Monitoring of Pipelines and Networks* (C. Verde & L. Torres, eds). Springer, pp. 13–37.

Zahab, S. E., Mosleh, F. & Zayed, T. 2016 An accelerometer-based real time monitoring and leak detection system for pressurized water pipelines. *Pipelines* 2016, Kansas City (MO).

Zielke, W. 1968 Frequency-dependent friction in transient pipe flow. *Journal of Basic Engineering* **90** (1), 109–115.

First received 30 April 2020; accepted in revised form 18 January 2021. Available online 1 February 2021